the quantity $\Delta S_m \Delta T$ is maximum. The RC values computed by the Wood and Potter method are shown in Fig. 4 as the rectangular areas overlapping and extending outside the shaded areas.

Received 2 December 2003; accepted 5 December 2004; doi:10.1038/nature02657.

1. Glanz, J. Making a bigger chill with magnets. *Science* **279,** 2045 (1998).
2. Tegus, O., Bruck, E., Buschow, K. H. J. & de Boer, F. R. Transition-metal-based refrigerants for room-temperature applications. *Nature* **415,** 150–152 (2002).
3. Tegus, O. *et al.* Magnetic-phase transitions and magnetocaloric effects. *Physica B* **319,** 174–192 (2002).
4. McMichael, R. D., Shull, R. D., Swartzendruber, L. J., Bennett, L. H. & Watson, R. E. Magnetocaloric effect in superparamagnets. *J. Magn. Magn. Mater* **111,** 29–33 (1992).
5. Fujita, A., Fujieda, S., Hasegawa, Y. & Fukamichi, K. Itinerant-electron metamagnetic transition and large magnetocaloric effects. *Phys. Rev. B* **67,** 104416 (2003).
6. Pecharsky, V. K. & Gschneidner, K. A. Jr The giant magnetocaloric effect in $Gd_5(Si_2Ge_2)$. *Phys. Rev. Lett.* **78,** 4494–4497 (1997).
7. Percharsky, A. O., Gschneidner, K. A. Jr & Pecharsky, V. K. The giant magnetocaloric effect of optimally prepared $G_5Ge_2Si_2$. *J. Appl. Phys.* **93,** 4722–4728 (2003).
8. Levin, E. M., Pecharsky, V. K. & Gschneidner, K. A. Jr Unusual magnetic behavior in $G_5(Ge_{1.5}Si_{2.5})$ and $G_5Ge_2Si_2$. *Phys. Rev. B* **62,** R14625–R14628 (2000).
9. Giguere, A. *et al.* Direct measurements of the 'giant' adiabatic temperature change in $G_5Ge_2Si_2$. *Phys. Rev. Lett.* **83,** 2262–2265 (1999).
10. Choe, W. *et al.* Making and breaking covalent bonds across the magnetic transition in the giant magnetocaloric material $Gd_5(Ge_2Si_2)$. *Phys. Rev. Lett.* **84,** 4617–4620 (2000).
11. Morellon, L., Algarabel, P. A., Ibarra, M. R., Blasco, J. & Garcia-Landa, B. Magnetic-field-induced structural transition in $Gd_5(Si_{1.8}Ge_{2.2})$. *Phys. Rev. B* **58,** R14721–R14724 (1998).
12. Meyers, J., Chumbley, S., Choe, W. & Miller, G. J. Microstructural analysis of twinned β-$G_5Ge_2Si_2$. *Phys. Rev. B* **66,** 012106 (2002).
13. Pecharsky, V. K. & Gschneidner, K. A. Jr Phase relationship and crystallography in pseudobinary system Gd_5Si_4-Gd_5Ge_4. *J. Alloys Compd.* **260,** 98–106 (1997).
14. Gschneidner, K. A. Jr, Pecharsky, V. K., Pecharsky, A. O. & Zimm, C. B. Recent development in magnetic refrigeration. *Mater. Sci. Forum* **315–317,** 69–76 (1999).
15. Wood, M. E. & Potter, W. H. General analysis of magnetic refrigeration and its optimization using a new concept: maximization of refrigerant capacity. *Cryogenics* **25,** 667–683 (1985).
16. Shull, R. D., Swartzendruber, L. J. & Bennett, L. H. in *Proc. Sixth Int. Cryocoolers Conf.* (eds Green, G. & Knox, M.) 231 (Publication no. DTRC-91/002, David Taylor Research Center, Annapolis, Maryland, 1991).
17. McMichael, R. D., Ritter, J. J. & Shull, R. D. Enhanced magnetocaloric effect in $Gd_3Ga_{5-x}Fe_xO_{12}$. *J. Appl. Phys.* **73,** 6946–6948 (1993).
18. Tishin, A. M. Magnetic refrigeration in the low-temperature range. *J. Appl. Phys.* **68,** 6480–6484 (1990).
19. von Ranke, P. J. *et al.* Anomalous magnetocaloric effect in YbAs associated with the giant quadrupolar interaction. *Phys. Rev. B* **63,** 24422 (2001).

Acknowledgements This work was partially supported by the NASA-Goddard Space Flight Center. We thank R. Waterstrat and R. Drew for technical assistance, and M. Lufaso and R. D. McMichael for helpful discussions.

Competing interests statement The authors declare that they have no competing financial interests.

Correspondence and requests for materials should be addressed to V.P. (virgil12@nist.gov).

Evidence for a macroscopic electric field in the sedimentation profiles of charged colloids

Mircea Raşa & Albert P. Philipse

Van 't Hoff Laboratory for Physical and Colloid Chemistry, Debye Institute, Utrecht University, Padualaan 8, 3584 CH Utrecht, The Netherlands

The determination of molecular masses from barometric sedimentation profiles, a main topic in ultracentrifugal analysis, is thought to be quantitatively correct for non-interacting particles[1,2]. Whereas this expectation is justified for uncharged colloids or macromolecules at low volume fractions, early ultracentrifugation studies[3] on charged particles had already indicated that the obtained masses might be much too low. More recently, expanded sedimentation profiles have been observed for charged particles[4,5], sometimes inflated by orders of magnitude[5] relative to the barometric prediction, which highlights a shortcoming in our understanding of centrifugation of even very dilute charged species[5]. Theory[6] and simulations[7], anticipated by various authors[4,8,9], now propose that strongly non-barometric sedimentation profiles might be caused by an internal macroscopic electric field that, even for non-interacting particles, significantly decreases the buoyant particle mass. The existence of this field and its intriguing consequences still lack experimental verification. Here we report ultracentrifugation experiments on charged colloidal silica spheres, showing both the existence of such a macroscopic electric field and its drastic effects on the sedimentation profiles of very dilute dispersions at low ionic strength.

Centrifugation is an indispensable technique for separating and analysing cells, organelles and macromolecules[1,2], as well as colloids[10]. A classical example is the centrifugation of DNA fragments in salt gradients, which confirmed the Watson–Crick model for DNA replication[11,12]. Absolute molecular masses can be determined directly under non-denaturating conditions from sedimentation–diffusion (SD) concentration profiles, a method reported to be rigorous[2]. The method assumes that, for sedimentation under gravity, the particle number density $\rho(x)$ at an altitude x in the SD profile follows from a Boltzmann distribution and has the form

$$\ln(\rho(x)) \propto -x/L \qquad (1)$$

In this 'barometric' profile, $L = k_B T/(mg)$ is the gravitational length for particles with buoyant mass m, T is the absolute temperature, k_B is the Boltzmann constant and g is the gravitational acceleration. It is generally assumed[10] that non-interacting particles will adopt such a barometric profile and that, consequently, sufficiently low concentrations ensure the validity of equation (1). Here, however, we report SD profiles of very dilute charged colloids that strongly deviate from the barometric distribution (equation (1)) owing to an electric field, which has only recently[6,7,13] been clearly identified as an important factor in the centrifugation of charged species.

Non-barometric behaviour due to an electric field is predicted to occur at sufficiently low ionic strength[6], and therefore we have studied the ultracentrifugation of well-defined, charged silica spheres (Table 1) in ethanol. This solvent is suitable because of its inherent low ionic strength and its ability to disperse charged silica spheres to non-aggregated 'alcosols' with practically unlimited colloidal stability[5,14,15]. We found that the centrifugated silica spheres form reproducible SD profiles that can be scanned with high spatial resolution (Fig. 1; see Methods section). SD profiles were studied for initial silica volume fractions down to 0.01% to minimize the effect of inter-particle interactions. We verified that the barometric part (region I; see below) of SD profiles yields a correct colloid radius: for a silica mass density of $1.6\,g\,cm^{-3}$ (Table 1), the measured centrifugal lengths correspond to a radius of 19.2 nm, which lies within the radius distribution determined from electron microscopy (Table 1). We also verified that uncharged silica spheres dispersed in cyclohexane yield the expected barometric profiles. However, for charged silica spheres all our experimental SD profiles, with a representative selection in Fig. 1, deviate drastically from the barometric distribution.

These deviations are due to a macroscopic electric field in the SD profile, that is, a gradient in an equilibrium electrical potential,

Table 1 **Properties of silica spheres (Labcode SiA) dispersed in ethanol**

R (nm)	σ (%)	R_h (nm)	δ (g cm^{-3})	μ (μm cm V^{-1} s^{-1})	z
21.9	11.6	30.0	1.6 ± 0.1	−0.95 ± 0.05	≈50

R and σ are radius and polydispersity, respectively, from transmission electron microscopy; R_h is the radius from dynamic light scattering; δ is the mass density from ref. 14; μ is the electrophoretic mobility for silica volume fractions in the range 0.01–0.3%; z is the number of elementary charges on silica particles, determined from electrophoretic mobility. Errors are ±s.d.

unrelated to the more familiar non-equilibrium streaming potentials or sedimentation potentials[10] generated by solvent motion relative to the colloids. The equilibrium field can be understood as a consequence of the huge mass difference between the (in our case negative) colloids and their positive counterions[6]. The practically weightless counterions attempt to achieve a homogeneous distribution in a sedimentation cell to maximize their entropy, whereas the heavy colloids accumulate near the cell bottom to minimize their gravitational potential energy. Electroneutrality, as has been pointed out[6], couples the two tendencies, causing an 'entropic lift' for the colloids, that is, an effective increase in their thermal energy corresponding to a decrease in the apparent colloid mass, which inflates the SD profile. The effect of added salt is to reduce the entropic lift or, equivalently, to weaken the electric field: when counterions diffuse upwards in a salt-free dispersion, only colloids are available as anionic chaperons to maintain electroneutrality. However, at higher ionic strength, molecular anions also accompany counterions, whereas at excess salt, charge separation is suppressed and the electric field vanishes.

To quantify this qualitative explanation and analyse the non-barometric SD profiles (Fig. 1) we extend equation (1) with an electrical term. The resulting non-barometric formula also follows from the classical Donnan membrane equilibrium for an inhomogenous colloidal solution[5,13]. Here we give an equivalent but more concise derivation. Consider a mixture of three species: colloids with charge z and number density ρ, monovalent cations with concentration c_+, and monovalent anions with concentration c_-. The dispersion is in thermodynamic equilibrium with an external salt reservoir with a total ion concentration of $2c_s$. The essential assumptions are that each separate species behaves ideally and that the three species jointly satisfy charge neutrality. For non-

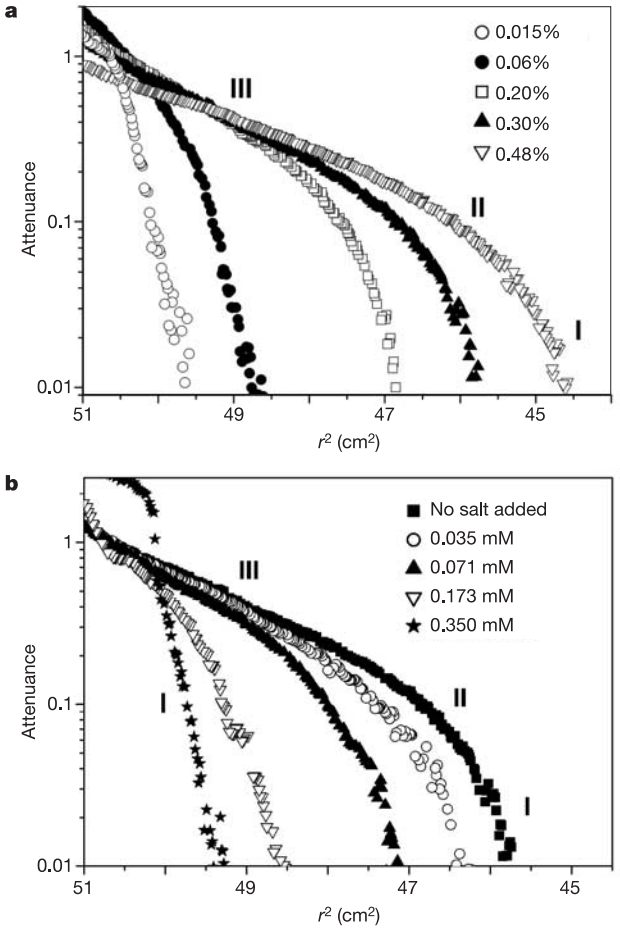

Figure 1 Experimental sedimentation–diffusion equilibrium profiles for dispersions of charged silica spheres in ethanol plotted as attenuance against the square of the radial distance from the centre of rotation. **a**, Representative profiles for dispersions having different initial volume fractions, with no added salt. Increase in the (very low) initial silica volume fraction significantly expands the exponential decay III as a consequence of the colloidal charge. **b**, Representative profiles for dispersions having a fixed initial silica volume fraction of 0.30%, at different salt concentrations. Increasing added amounts of $LiNO_3$ gradually compress the profile towards the barometric distribution I.

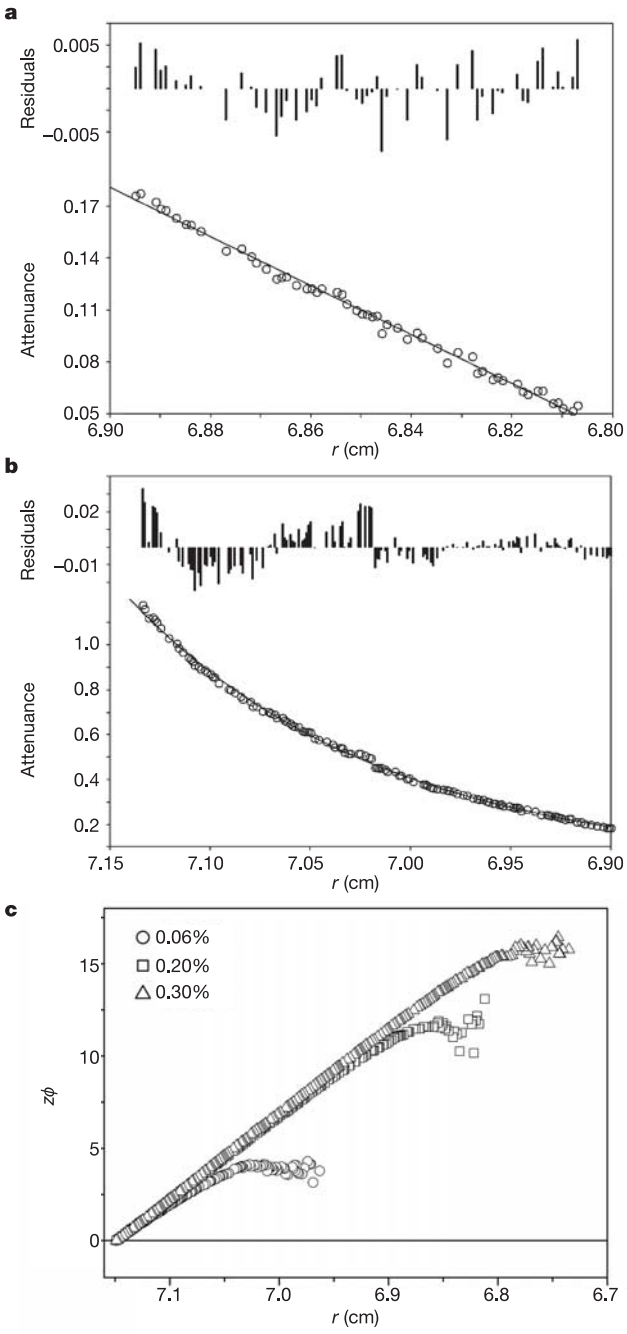

Figure 2 Analysis of the experimental profiles from Fig. 1a. **a**, An example of a nearly perfect quadratic fit to the data extracted from region II of the 0.30% sample, which clearly confirms the peculiar decay predicted for region II (see the text and Methods). **b**, An example of a nearly perfect exponential fit to the data extracted from region III of the same sample, resulting in a different centrifugal length from that of region I. **c**, Non-dimensional electrical potential times z plotted against the radial distance for three initial volume fractions of particles.

interacting, weightless ions, thermodynamic equilibrium requires the gradient in their osmotic pressure to balance the force (per volume) exerted on the ions by the internal electric field E:

$$-k_B T(\mathrm{d}c_\pm/\mathrm{d}x) \pm ec_\pm E = 0 \quad (2)$$

Here e is the proton charge; the electrostatic potential ψ follows from $E = -\mathrm{d}\psi/\mathrm{d}x$. The boundary condition on equation (2) is that $c_+ = c_- = c_s$ in the reservoir where $\psi = 0$. For the much heavier colloids the equilibrium condition contains the gravitational force per volume:

$$-k_B T(\mathrm{d}\rho/\mathrm{d}x) - ze\rho E - m\rho g = 0 \quad (3)$$

again assuming non-interacting particles. The electric field term always accompanies the gravitational field term and vanishes only if gravity is switched off. To find the non-barometric SD profile from equation (3) one more equation is needed, for which we use here the macroscopic neutrality condition

$$-z\rho + c_+ - c_- = 0 \quad (4)$$

Integrating equation (2) yields the ion concentration profiles c_+ and c_-. Substituting them in equation (4) and combining the result with equation (3) finally yields the SD profile

$$\ln(y) + z\,\mathrm{arcsinh}(y) = -(x/L) + C \quad (5)$$

Here $y = z\rho/(2c_s)$ is a non-dimensional number density of colloids and C is an integration constant determined by the total number of colloids[13]. The reduced electrical potential $\phi = e\psi/(k_B T)$ is, according to equation (4), given by $\phi = -\mathrm{arcsinh}(y)$. The difference between the profiles in equations (1) and (5) is not merely adding the electrical work term; there is always an electrical field E opposing gravity whenever $z > 0$ (for explicit expressions of E see ref. 13). The homogeneous electric field E in regions II and III (see below) is expected to have a strength of order $E \approx mg/(ez)$. These two regions can be regarded as a macroscopic condenser[6,13] resulting from the charge separation that produces the equilibrium macroscopic field. Note that equations (1) and (5) are one-dimensional SD profiles in the gravitational field; for profiles in the radial field of an ultracentrifuge see Methods. For $zy \ll 1$ (region I), equation (5) asymptotes to the barometric exponential (equation (1)), whereas for $y \gg 1$ (region III) the profile also decays exponentially, as $\ln(y) \sim -x/((z+1)L)$, but with an inflated gravitational length of $(z+1)L$ corresponding to a strongly reduced effective mass. Our experiments (Fig. 1) clearly show both exponential regions in one and the same SD profile. Moreover, when salt is added to decrease the average value of y, the barometric region I grows at the expense of region III, which eventually disappears (Fig. 1b). This marked salt effect confirms equation (5) and previous calculations[6]. Note that in Fig. 1b only little salt is needed to change SD profiles substantially. Without added salt, incidentally, the ion concentration, estimated from electrical conductivity measurements, is only of the order of 10^{-5} M, corresponding to a Debye screening length of about 30 nm.

In addition to the two exponential regions, a linear concentration decay is predicted[6] in an intermediate region II, characterized by a low colloid density ($y \ll 1$) and a high counterion density ($zy \gg 1$), inequalities for which equation (5) indeed yields the linear asymptote: $\mathrm{arcsinh}(y) \sim y = 1 - x/(zL)$ (in the centrifugal field this decay is quadratic; see Methods). This most unusual SD profile, ascribed to a near cancellation of gravity by the electric field[6], is quite narrow unless z is very large. The silica sphere charge is only $z \approx 50$ (see Methods), but owing to the high resolution in our SD profiles a zoom-in (Fig. 2a) nevertheless clearly reveals the region II.

Equation (5) implies a significant rescaling of SD profiles, by extracting the barometric part (region I) from the experimental SD profiles to obtain $z\phi$ as a function of altitude. The results (Fig. 2c) show unambiguously the presence of a macroscopic electric field in a substantial part of SD profiles. The electrical potential decreases with the radial distance r and flattens on entering region I towards the constant electrical potential of the background electrolyte depleted of colloids. The largest overall potential jump in Fig. 2c is about 8 mV for $z \approx 50$, which agrees in order of magnitude with electrochemical Donnan potential measurements on silica dispersions in ethanol, with comparable differences in concentrations as in the SD profiles (B. Erné, unpublished observations). The slope $z\mathrm{d}\phi/\mathrm{d}r$ in Fig. 2c is proportional to the electrical force on colloids, which indeed almost compensates for the buoyant mass: for our silica spheres, the experimental slope (46.6 cm^{-1}) corresponds to a ratio of the electric force zeE to the centrifugal force $m\omega^2 r$ very close to unity. Note that for this calculation we do not need the value of z.

The applicability of equation (5) is noteworthy because it disregards all colloid–colloid and ion–ion correlations as well as electrical potential variations on the scale of colloids and ions. One would expect deficiencies in this model to show up in the more concentrated part of the profile (region III). We found for some of the profiles in Fig. 1a that the exponential decay in region III extends over a wider spatial range than predicted by equation (5). Moreover, a fit to region III (Fig. 2b) using the appropriate radial SD profile (see Methods) yields $z \approx 4$–8 (Table 2). These values of z are low in comparison with values estimated from region II (Table 2) and electrophoresis (Table 1), which agree very well at lower volume fractions. Clearly, an extension of the theory beyond equation (5) is needed to further clarify the SD profiles at low altitude. This extension does not necessarily involve colloidal interactions (which might contribute to non-barometric behaviour): in our SD profiles these interactions have a much smaller effect than the electric field. We verified this by numerical calculations of the osmotic second virial coefficient for colloids interacting by means of an electrical double-layer repulsion[5,10]: for concentrations in region III, the first-order correction in the virial expansion of the osmotic pressure is much smaller than the total pressure exerted by non-interacting colloids and their counterions. This confirms that also in region III the electric field is the dominant cause of non-barometric behaviour.

Thus, we have experimentally demonstrated the existence of a macroscopic electric field, producing strongly non-barometric SD profiles of charged colloids. The unusual shape of experimental SD profiles and the marked effect of added salt validate equation (5), which is based only on the assumptions of ideal species and charge neutrality. This simple model, which explains our results surprisingly well, nevertheless needs extension to quantify region III better. Although our experiments relate to charged silica spheres, it is clear that non-barometric behaviour can occur for any type of sedimenting charged species. In this respect it should be noted that the mass determination of biomolecules by centrifugal analysis at excess salt, to suppress charge effects, certainly makes sense in the light of our findings. However, our work shows clearly that an excess of salt also suppresses important information on the electrical properties of macromolecules: centrifugal analysis of polyelectrolytes at low salt concentration still provides the molecular mass (region I), but in principle also yields their valency and the macroscopic electrostatic potential that they generate in solution. It would be interesting to (re)examine the sedimentation of polyelectrolytes such as DNA or proteins from this perspective. □

Table 2 **Results of fit analysis of profiles presented in Fig. 1a**

Volume fraction (%)	$L_{\omega,\mathrm{I}}$ (cm)	z_{II}	z_{III}
0.06	0.37	45	4
0.20	0.39	55	4
0.30	0.39	65	5
0.48	0.37	80	8

$L_{\omega,\mathrm{I}}$ is the centrifugal length, determined from region I; z_{II} is the number of elementary charges on particles, determined from region II; z_{III} is the number of elementary charges on particles, determined from region III.

Methods

Silica dispersions

Amorphous silica spheres (Table 1) were synthesized by polymerization of (hydrolysed) tetraethoxysilane in an ethanol–ammonia mixture[14,15]. The silica surface was modified by covalent reaction with 3-methacryloxypropyltrimethoxysilane (TPM) during distillation, simultaneously transferring the silica spheres to absolute (analytical grade) ethanol. The stock dispersion for the ultracentrifugation experiments was free from contaminants such as polymeric species or secondary silica particles, which might have affected SD profiles[5]. TPM-coated silica spheres do not aggregate in ethanol and are well documented model particles for the study of charge-stabilized colloids[15,16]. Particle characterization (Table 1) was performed on the same samples as used for ultracentrifugation.

Ultracentrifugation

Ultracentrifugation was performed with a Beckman Optima XL-A analytical ultracentrifuge, in accordance with the manufacturer's instruction manual, in sector-shaped sedimentation cells thermostatically controlled at 298 K. The optical system measures the transmittance, H, of the sample against a reference of pure ethanol or salt solution and the results are converted to the attenuance $A = \ln(1/H)$ as plotted in Fig. 1. The attenuance is linearly proportional to the number density of silica particles up to a silica volume fraction of 2.5%, as checked with light attenuation (extinction) measurements. A silica sphere radius of about 22 nm was convenient for achieving profiles of sufficient thickness, which nevertheless decay fully within the available (radial) space to the solvent depleted of particles (within the limits of the sensitivity of the instrument). SD equilibrium was achieved on a time scale of up to 7 days at low rotor speeds (1100 r.p.m., corresponding to an acceleration of 88 g in the centre of the cell). Homogenization and recentrifugation of the same cell content reproduced the SD profiles very well, which also confirms that the silica spheres do not aggregate in the centrifugal field. The radial centrifugal field requires a modification of equation (5):

$$\ln(y) + z\,\mathrm{arcsinh}(y) = (r^2 - r_b^2)/(2L_\omega^2) + C \qquad (6)$$

Here r is the radial distance from the rotor axis, r_b denotes the cell bottom and L_ω is the centrifugal length. The three regions are now characterized by the following equations: $\ln(y) \sim C_1 + (r^2 - r_1^2)/(2L_\omega^2)$ (region I), $y \sim C_2 + c_s(r^2 - r_1^2)/(z^2L_\omega^2)$ (region II) and $\ln y \sim C_3 + (r^2 - r_b^2)/[2(z+1)L_\omega^2]$ (region III), where r_1 is the crossover between the first two regions. SD profiles were always fitted with these quadratic arguments, although the experimental profiles are narrow so that they are very close to those formed in gravitational field (see, for example, Fig. 2a). For the radial electric field corresponding to equation (6) see ref. 13. The initial volume fractions of the homogeneous samples subjected to ultracentrifugation varied from 0.01% to 0.5%; after the SD equilibrium was reached, the altitude-dependent volume fraction of particles shows, at the bottom of profiles, values 7-fold down to 4-fold the initial values, respectively.

Electrophoretic mobility and electrical conductivity

Electrophoretic mobility and electrical conductivity were measured with a DELSA 440SX (Coulter) at 298 K for all samples. The mobility was determined from a Lorentzian fit to the measured peaks at four scattering angles and was further used to estimate the charge z of the particles in the frame of the Debye–Hückel model with a previously reported method[17]. Conductivities obtained from the DELSA were used to estimate the ion particle number density by the method of ref. 17. We found a negligible dependence of the mobility on sample volume fraction; that is, the measured values for all samples were $-0.95 \pm 0.5\,\mu m\,cm\,V^{-1}\,s^{-1}$ (mean ± s.d.). The conductivity increased weakly with the volume fraction of particles, being in the range 1.4–2.9 $\mu S\,cm^{-1}$.

Received 30 March; accepted 4 May 2004; doi:10.1038/nature02672.

1. Harding, S. E., Rowe, A. J. & Horton, J. C. (eds) *Analytical Ultracentrifugation in Biochemistry and Polymer Science* (Royal Society of Chemistry, Cambridge, 1993).
2. Stryer, L. *Biochemistry*, 4th edn (Freeman, New York, 1995).
3. Svedberg, T. & Pederson, O. *Die Ultrazentrifuge* (Dresden, 1940).
4. Piazza, R., Bellini, T. & Degiorgio, V. Equilibrium sedimentation profiles of screened charged colloids: a test of the hard-sphere equation of state. *Phys. Rev. Lett.* **71,** 4267–4270 (1993).
5. Philipse, A. P. & Koenderink, G. H. Sedimentation-diffusion profiles and layered sedimentation of charged colloids at low ionic strength. *Adv. Colloid Interface Sci.* **100–102,** 613–639 (2003).
6. Van Roij, R. Defying gravity with entropy and electrostatics: sedimentation of charged colloids. *J. Phys.: Condens. Matter* **15,** S3569–S3580 (2003).
7. Hynninen, A. P., Van Roij, R. & Dijkstra, M. Sedimentation profiles of charged colloids: Entropic lift and charge separation. *Europhys. Lett.* **65,** 719–725 (2004).
8. Biben, T. & Hansen, J. P. Sedimentation equilibrium in concentrated charged–stabilized colloidal suspensions. *J. Phys.: Condens. Matter* **6,** A345–A349 (1994).
9. Löwen, H. The apparent mass in sedimentation profiles of charged suspensions. *J. Phys.: Condens. Matter* **10,** L479–L485 (1998).
10. Hunter, R. J. *Foundations of Colloid Science* Vol I (Clarendon, Oxford, 1991).
11. Becker, W. M., Kleinsmith, L. J. & Mardin, J. *The World of the Cell* (Benjamin Cummins, San Francisco, 2000).
12. Meselson, M. & Stahl, F. W. The replication of DNA in *Escherichia coli*. *Proc. Natl. Acad. Sci. USA* **44,** 671–682 (1958).
13. Philipse, A. P. Remarks on the Donnan condenser in the sedimentation–diffusion equilibrium of charged colloids. *J. Phys.: Condens. Matter* (submitted).
14. Philipse, A. P. & Vrij, A. Preparation and properties of nonaqueous model dispersions of chemically modified charged silica spheres. *J. Colloid Interf. Sci.* **128,** 121–153 (1989).
15. Philipse, A. P. & Vrij, A. Determination of static and hydrodynamic interactions between monodisperse silica spheres in an optically matching, organic solvent. *J. Chem. Phys.* **88,** 6459–6470 (1988).
16. Thies-Weesie, D. M. E., Philipse, A. P., Nägele, G., Mandl, B. & Klein, R. Non-analytical concentration dependence of sedimentation of charged silica spheres in an organic solvent. Experiments and calculations. *J. Colloid Interf. Sci* **176,** 43–54 (1995).
17. Rasa, M., Philipse, A. P. & Meeldijk, J. D. Heteroaggregation, repeptisation, and stability in mixtures of oppositely charged colloids. *J. Colloid Interf. Sci.*(in press).

Acknowledgements We thank R. van Roij and G. Koenderink for discussions and collaboration, B. Erné for sharing insights and unpublished results on Donnan potentials, N. Zuiverloon for synthesizing the silica spheres, and D. Thies-Weesie for maintenance of the ultracentrifuge. This work was supported financially by The Netherlands Organization for Scientific Research (NWO/Stichting Chemische Wetenschappen).

Competing interests statement The authors declare that they have no competing financial interests.

Correspondence and requests for materials should be addressed to A.P.P. (a.p.philipse@chem.uu.nl).

Role of CO_2 in the formation of gold deposits

G. N. Phillips[1] **& K. A. Evans**[2]

[1]*CSIRO Division of Exploration and Mining, PO Box 3, Central Park, Victoria 3145, Australia*
[2]*CSIRO Division of Exploration and Mining, School of Geosciences, Building 28, Monash University, Victoria 3800, Australia*

Much of global gold production has come from deposits with uneconomic concentrations of base metals, such as copper, lead and zinc[1]. These 'gold-only' deposits are thought to have formed from hot, aqueous fluids rich in carbon dioxide[2], but only minor significance has been attached to the role of the CO_2 in the process of gold transport. This is because chemical bonding between gold ions and CO_2 species is not strong[3], and so it is unlikely that CO_2 has a direct role in gold transport. An alternative indirect role for CO_2 as a weak acid that buffers pH has also appeared unlikely, because previously inferred pH values for such gold-bearing fluids are variable[2,4,5,6]. Here we show that such calculated pH values are unlikely to record conditions of gold transport, and propose that CO_2 may play a critical role during gold transport by buffering the fluid in a pH range where elevated gold concentration can be maintained by complexation with reduced sulphur. Our conclusions, which are supported by geochemical modelling, may provide a platform for new gold exploration methods.

The world's major gold-only deposits have formed by precipitation of gold from aqueous fluids migrating on a kilometre-scale through the bedrock that comprises the upper part of the Earth's crust. These fluids show a remarkably consistent set of characteristics. They are at temperatures above 200 °C, rich in CO_2 (up to 20–30 mol%; Table 1), sulphur-bearing, low salinity compared to most ore-bearing fluids, and have a redox state more reducing than the haematite–magnetite buffer such that the sulphur is predominantly in the reduced state[1]. These characteristics have been confirmed (by techniques including fluid-inclusion and stable-isotope analyses) for deposit types that account for the bulk of the world's gold production, both today and historically—for example, Archaean greenstone gold[2,7], slate-belt gold[8], the Mother Lode of California[6], gold in banded iron formations[2], Carlin-type gold[9] and the Witwatersrand goldfields[9,10].

With the exception of the high CO_2 concentrations, these shared fluid characteristics can be explained by the chemical attributes of the dissolved gold. The somewhat reducing fluids and elevated temperatures favour the ionic state of Au^+ for the gold in solution[3].